CHAPTER 5

Image Analysis by Fractional-order Orthogonal Moments

O. El ogri, M. Yamni, H. Karmouni, A. Daoui, M. Sayyouri and H. Qjidaa

Continuous orthogonal moments and discrete orthogonal moments, as a category of typical moments, have been widely used in image analysis. However, the order of these moments is limited to an integer and their fractional versions have not been studied sufficiently in the literature. This chapter provides an overview of fractional order orthogonal moments (FrOM) and their applications in image analysis. A detailed study of these moments is provided, including the mathematical development, properties, and computational aspects of these descriptors. Applications have been

O. El ogri, M. Yamni, H. Karmouni, H. Qjidaa
CED-ST, STIC, Laboratory of Electronic Signals and Systems of Information LESSI,
Faculty of Science Dhar El Mahrez, University Sidi Mohamed Ben Abdellah,
Fez, Morocco
e-mail: {omar.elogri,mohamed.yamni,hicham.karmouni,hassan.qjidaa}@usmba.ac.ma

A. Daoui, M. Sayyouri
Engineering, Systems and Applications Laboratory,
National School of Applied Sciences, Sidi Mohamed Ben Abdellah University,
BP 72, My Abdallah Avenue Km. 5 Imouzzer Road,
Fez, Morocco
e-mail: {achraf.daoui, mhamed.sayyouri}@usmba.ac.ma

Editor: G.A. Papakostas, *Recent Progress in Image Moments and Moment Invariants*
DOI: 10.15579/gcsr.vol7.ch5, GCSR Vol. 7, pp. 101-131, 2022

studied to validate the performances of the presented FrOMs, such as 2D/3D image reconstruction, RST invariance, 2D/3D image classification and image watermarking. The theoretical analysis and the experimental results show the superiority and the efficiency of the FrOMs compared to the classical versions in terms of the results obtained in the adopted image processing applications.

5.1 Introduction

Moments are important image descriptors in computer vision. They have been widely used in many applications such as image analysis [37, 57, 56, 21], image reconstruction [61, 10, 22], image watermarking [35, 51, 53], image compression [38, 50], medical image analysis [9], image registration, texture retrieval [8], image indexing [36], edge detection, template matching [18], face recognition [14, 12], 3D geometric [28, 27, 23], optical flow estimation [32] and forgery detection [42].

Generally, moments are divided into two main categories: (1) non-orthogonal moments and (2) orthogonal moments [13]. Geometric moments are the most popular moments in the first category because they are the first that have been applied for image analysis due to their simplicity. However, they suffer from the problem of information redundancy due to the non-orthogonality of their kernel function, which limits their applications in cases where more discriminating information must be captured [52]. This problem led scientists to introduce the second category of moments, Orthogonal Moments (OMs), which use orthogonal polynomials as kernel functions. Thanks to the orthogonality property, OMs are able to represent images without information redundancy and therefore have attracted considerable attention in several applications relating to images and signals. OMs also fall into two main families: Continuous Orthogonal Moments (COMs) which are based on continuous orthogonal polynomials such as Legendre [48], Zernike [33], pseudo-Zernike [7], Gegenbauer [19], Jacobi, Fourier-Mellin [46], Gaussian-Hermite [54], Chebyshev [59] and separable COMs [59], as long as the Discrete Orthogonal Moments (DOMs) which are based on discrete orthogonal polynomials such as the polynomials of Tchebichef [37], Krawtchouk [57], [26], Hahn [56], Charlier [60, 16], Meixner [45, 25], Dual Hahn [62], Racah [61] and separable DOMs [59, 44, 43, 17].

A thorough literature study has shown that the order of the existing orthogonal moments (COMs and DOMs) is always limited to an integer, because the kernel function is defined for the integer order. However, it is sometimes necessary to calculate them for real or fractional orders for reasons of accuracy, security and location of Regions of Interest (ROI) in the image. In recent years, the focus has been on the search for fractional OMs (FrOMs). In this direction, some continuous FrOMs (FrCOMs) have been proposed, namely the fractional moments of Fourier-Mellin (FrFMMs) [58], Legendre (FrLMs) [49], Zernike (FrZMs) [30], Chebyshev (FrChMs) [5] and generalized Laguerre [11]. The FrCOMs are defined by substituting x by x^{α} ($\alpha \in R^{+}$) in the kernel function of conventional moments. Therefore, the order of the FrCOMs becomes a positive real number.

Since the images are discrete, the calculation of FrCOMs is characterized by [24]: 1) the need for an appropriate transformation of the image coordinates for FrCOMs to

be applied, and by 2) the approximation of the integrals by summations, which causes discretization and approximation errors. To limit these errors, scientists are oriented towards Fractional Discrete Orthogonal Moments (FrDOMs) such as the FrDOMs of Krawtchouk (FrKMs) [35], Tchebichef (FrTMs) [51] and Charlier (FrCMs) [53]. Since the substitution method (x by x^{α}) cannot be applied to the case of discrete moments, the derivation of the FrDOMs is done by the decomposition of the eigenvalues of the matrix of the classical kernel function. FrDOMs have the particularity of being directly defined in the discrete image domain, which has established them as families of moments with high discriminating power. FrCOMs and FrDOMs can be considered as a general version of classical COMs and DOMs, respectively.

In this chapter, we present a detailed overview of the properties of FrCOMs and FrDOMs and their applications in the image field.

In the first axis of this chapter, we discuss in detail the properties of FrCOMs and provide a detailed discussion of the computational aspects of these descriptors, including mathematical development fast and stable accurate computation. The FrCOMs of Legendre (FrLMs) are implemented in this chapter as an example of this type of moments. The capacity of FrLMs is evaluated in terms of 2D/3D image reconstruction, RST invariance and 2D/3D image classification.

In the second axis of this chapter, we discuss in detail the properties of FrDOMs and then present the mathematical background of FrDOM theory, including algebraic development and the properties of eigenvalues and eigenvectors of the kernel function. To illustrate the application of FrDOMs, a watermarking scheme for image copyright protection is studied. The Fractional Charlier moments (FrCMs) are implemented to show the interest of this type of moments and the advantages that can be expected through an appropriate choice of fractional orders. Several numerical experiments are performed to confirm the effectiveness of FrDOMs in terms of imperceptibility, robustness, and security of watermarking scheme.

The theoretical analysis and the experimental results show the superiority and the efficiency of the FrOMs (FrCOMs and FrDOMs) compared to the classical versions in terms of the results obtained in the adopted image processing applications.

5.2 Fractional-order Continuous Orthogonal Moments (FrCOMs)

Orthogonal moments are the most prominent global shape descriptors which are widely used for various image processing and computer vision applications such as image classification, object recognition, image retrieval. However, the continuous orthogonal moments and their Rotation, Scaling and Translation (RST) invariants are restricted to being an integer order, where the order of the basis continuous orthogonal polynomials are integers. Consequently, less work has been carried out in the literature for the use of fractional-order continuous orthogonal moments (FrCOMs) as shape descriptors for 2D and 3D images classification. Orthogonal moments with integer-order are a special case of fractional-order orthogonal moments.

In recent years, considerable attention has been given to find more accurate numerical solution of Fractional Differential Equations (FDEs) using continuous orthogonal

polynomials. In fact, the numerical resolution of fractional differential equations from orthogonal polynomials requires the definition of a new type of orthogonal polynomials, called Fractional-order orthogonal polynomials [31, 29]. This type of orthogonal polynomials involves the introduction of a fractional parameter $\alpha \succ 0$, in order to generalize the notion of integer order n with $n \in N$ to the fractional order $n\alpha$. This has led to define the fractional-order type of some classical orthogonal moments [59, 20, 34, 55], such as fractional-order Legendre moments [49], fractional-order Zernike moments [30], fractional-order Chebyshev moments [5] and fractional-order generalized Laguerre moments [11].

In the following, we present the concept of fractional orthogonal moments and discussed their properties while applying them on 2D and 3D image reconstruction and object recognition. We initially introduce the necessary relations and properties to define the FrLMs in the Cartesian coordinates. Then, we provide the theoretical framework to construct the Fractional-order Legendre Moment Invariants (FrLMIs), which are invariants with respect to rotation, scaling and translation transforms. After extensive experimentation, it is found that fractional moments are highly robust to image noise, capable of ROI feature extraction and are better than conventional integer order moments in both image reconstruction and classification of 2D and 3D images.

5.2.1 Classical Orthogonal Legendre polynomials

The classical orthogonal Legendre polynomials of integer order [41], which denoted as $L_n(x)$, are a set of orthogonal polynomials on the interval $[-1, 1]$. These polynomials, $L_n(x)$, satisfy the condition:

$$\int_{-1}^{1} L_n(x) L_m(x)\, w(x)\, dx = d_n^2 \delta_{nm}, \tag{5.1}$$

with respect to the weight function $w(x) = 1$ and the squared norm $d_n^2 = \frac{2}{2n+1}$, where δ_{nm} denotes the Kronecker symbol.

Legendre polynomials defined in Cartesian coordinates, which are called Shifted Legendre polynomials (SLPs) can be easily obtained by the three terms recurrence formula:

$$\begin{aligned} &L_{n+1}(x) = \tfrac{(2n+1)(2x-1)}{n+1} L_n(x) - \tfrac{n}{n+1} L_{n-1}(x) \quad ; \quad n \geq 1 \\ &L_0(x) = 1, \quad L_1(x) = 2x - 1. \end{aligned} \tag{5.2}$$

The analytic form of the shifted Legendre polynomial $L_n(x)$ of degree n given by

$$L_n(x) = \sum_{k=0}^{n} (-1)^{n+k} \begin{pmatrix} n \\ k \end{pmatrix} \begin{pmatrix} n+k \\ k \end{pmatrix} x^k. \tag{5.3}$$

Note that $L_n(0) = (-1)^n$ and $L_n(1) = 1$.

5.2.2 Fractional-order Orthogonal Legendre Polynomials

Let α be a rational positive number $\alpha \succ 0$. The Fractional-order Orthogonal Legendre Polynomials (FrLPs), denoted $FrL_n^\alpha(t)$, are defined on the interval $[0,1]$ and can be determined by introducing the change of variable $x = 2\,t^\alpha - 1$, we can define the fractional-order Legendre polynomials $FrL_n^\alpha(t)$ as [31, 29]:

$$FrL_n^\alpha(t) = L_n(2t^\alpha - 1), t \in [0,1]\,. \tag{5.4}$$

The FrLPs are a particular solution of the normalized eigenfunctions of the singular Sturm–Liouville problem [31]:

$$\left[(t - t^{1+\alpha}) FrL_n'^{\,\alpha}(t)\right]' + \alpha^2 n(n+1) t^{\alpha-1} FrL_n^\alpha(t) = 0, \;\; t \in [0,1]\,. \tag{5.5}$$

By using the recurrence formula of Eq.(5.2), we can define the three terms recurrence formula of the FrLPs as:

$$\begin{aligned} &FrL_{n+1}^\alpha(t) = \tfrac{(2n+1)(2t^\alpha-1)}{n+1} FrL_n^\alpha(t) - \tfrac{n}{n+1} FrL_{n-1}^\alpha(t) \quad ; \quad n \geq 1 \\ &FrL_0^\alpha(t) = 1, \quad FrL_1^\alpha(t) = 2t^\alpha - 1. \end{aligned} \tag{5.6}$$

The FrLPs satisfy the orthogonality relation on the interval $[0,1]$:

$$\int_0^1 FrL_n^\alpha(t) FrL_m^\alpha(t)\, w_\alpha(t)\, dt = d_{n,\alpha}^2 \delta_{nm}, \tag{5.7}$$

with respect to the weight function $w_\alpha(t) = t^{\alpha-1}$ and the squared norm $d_{n,\alpha}^2 = \frac{1}{\alpha(2n+1)}$.

The analytic form of $FrL_n^\alpha(t)$ of degree $n\alpha$ given by

$$FrL_n^\alpha(t) = \sum_{k=0}^{n} B_{nk} t^{\alpha k}, with B_{nk} = (-1)^{n+k} \left(\begin{array}{c} n \\ k \end{array} \right) \left(\begin{array}{c} n+k \\ k \end{array} \right). \tag{5.8}$$

We can define the normalized FrLPs by:

$$\widetilde{FrL}_n^{\,\alpha}(t) = \sqrt{\frac{w_\alpha(t)}{d_{n,\alpha}^2}} FrL_n^\alpha(t). \tag{5.9}$$

Therefore, the orthogonality relation of the normalized FrLPs is given by:

$$\int_0^1 \widetilde{FrL}_n^{\,\alpha}(t) \widetilde{FrL}_m^{\,\alpha}(t) dt = \delta_{nm}. \tag{5.10}$$

Figure 5.1(a), (b), (c) and (d) show the plots for the first seven orders of the fractional-order Legendre polynomials $FrL_n^\alpha(t)$ in the interval $[0,1]$, for different values of $\alpha = 0.2$, $\alpha = 1$, $\alpha = 1.4$ and $\alpha = 3$, respectively.

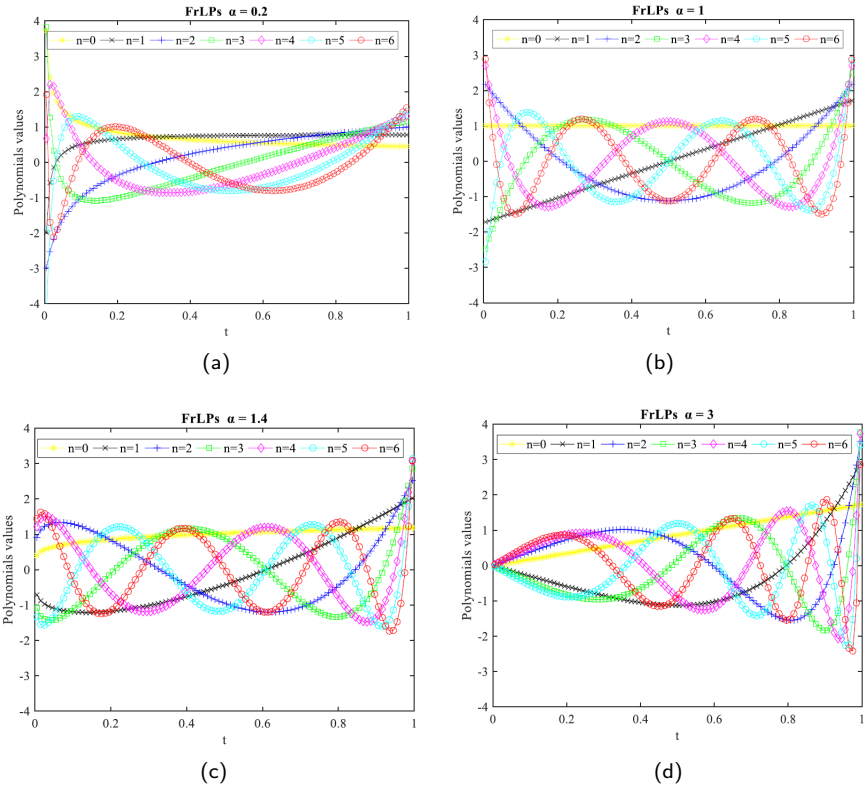

Figure 5.1: Plot of FrLPs for different values of $\alpha = 0.2$, $\alpha = 1$, $\alpha = 1.4$ and $\alpha = 3$ up to order 6, with $t \in [0, 1]$.

Unlike the classical orthogonal Legendre polynomials of integer order, which possess a uniform distribution of zeros at fixed points, the FrLPs provide the capability to control the distribution of zeros and their positions, based on the fractional parameter α. As demonstrated in Figure 5.1, for $\alpha = 1$, we can recover the classical shifted Legendre polynomials, and therefore the zeros are uniformly distributed on the definition interval. On the other hand, by taking $\alpha \prec 1$, the distribution of zeros of FrLPs is biased to the left region of the interval $[0, 1]$. While, for $\alpha \succ 1$, the distribution of zeros of FrLPs is biased to the right region of the interval $[0, 1]$. Finally, a more profound understanding of the FrLPs can be found in the study [31, 29].

5.2.3 Fractional-order Orthogonal Legendre Moments

The Fractional-order Orthogonal Legendre Moments (FrLMs) of order $\alpha(n + m + p)$ with $n, m, p \in \mathrm{N}$ for a given function $f(x, y, z)$, which is defined continuously on the square region $[0, 1] \times [0, 1] \times [0, 1]$ can be computed using the continuous integrals as follows:

$$FrLM^{\alpha}_{nmp} = \int_0^1 \int_0^1 \int_0^1 f(x, y, z)\widetilde{FrL}_n^{\alpha_x}(x)\widetilde{FrL}_m^{\alpha_y}(y)\widetilde{FrL}_p^{\alpha_z}(z)dxdydz. \quad (5.11)$$

Hence, for a digital image intensity function $f(i, j, k)$ of size $N \times M \times K$, the moments $FrLM^{\alpha}_{nmp}$ can be computed using ZOA method as:

$$FrLM^{\alpha}_{nmp} = \sum_{i=0}^{N-1}\sum_{j=0}^{M-1}\sum_{k=0}^{K-1} f(i, j, k)\widetilde{FrL}_n^{\alpha_x}(x_i)\widetilde{FrL}_m^{\alpha_y}(y_j)\widetilde{FrL}_p^{\alpha_z}(z_k)\Delta_x\Delta_y\Delta_z, \quad (5.12)$$

with $\Delta_x = \frac{1}{N}$, $\Delta_y = \frac{1}{M}$ and $\Delta_z = \frac{1}{K}$, where the mapped image coordinates are: An approximation of the original image can be reconstructed by:

$$f(i, j, k) = \sum_{i=0}^{n_{\max}}\sum_{j=0}^{m_{\max}}\sum_{k=0}^{p_{\max}} FrLM^{\alpha}_{nmp}\widetilde{FrL}_n^{\alpha_x}(x_i)\widetilde{FrL}_m^{\alpha_y}(y_j)\widetilde{FrL}_p^{\alpha_z}(z_k). \quad (5.13)$$

The fractional values α_x, α_y and α_z are used to control the distribution of zeros, allowing the capacity to extract local shape features from any Region-Of-Interest (ROI) of the image [49, 11], which makes the moments more suitable for image matching and local image watermarking. In fact, FrLMs can be used for ROI feature extraction in image analysis.

5.3 Fractional-order Legendre Moment Invariants

5.3.1 Fractional-order Geometric Moment Invariants

The Geometric Moments of fractional-order (FrGMs), $(\alpha_x p+\alpha_y q+\alpha_z r)$ for the image function, $f(i, j, k)$, of the size $N \times M \times K$, are defined as follows:

$$FrGM_{pqr}^{\alpha_x\alpha_y\alpha_z} = \sum_{i=0}^{N-1}\sum_{j=0}^{M-1}\sum_{k=0}^{K-1} f(i,j,k) m_{pqr}^{\alpha_x\alpha_y\alpha_z}(x_i,y_j,z_k), \tag{5.14}$$

where

$$m_{pqr}^{\alpha_x\alpha_y\alpha_z}(x_i,y_j,z_k) = \int_{x_i-\frac{\Delta x_i}{2}}^{x_i+\frac{\Delta x_i}{2}} \int_{y_i-\frac{\Delta y_j}{2}}^{y_i+\frac{\Delta y_j}{2}} \int_{z_k-\frac{\Delta z_k}{2}}^{z_k+\frac{\Delta z_k}{2}} x^{\alpha_x p} y^{\alpha_y q} z^{\alpha_z r} dxdydz. \tag{5.15}$$

Therefore, based on the separability property of the moments kernel function, we can write the triple integral as follow:

$$m_{pqr}^{\alpha_x\alpha_y\alpha_z}(x_i,y_j,z_k) = \left(\int_{x_i-\frac{\Delta x_i}{2}}^{x_i+\frac{\Delta x_i}{2}} x^{\alpha_x p} dx\right)\left(\int_{y_i-\frac{\Delta y_j}{2}}^{y_i+\frac{\Delta y_j}{2}} y^{\alpha_y q} dy\right)\left(\int_{z_k-\frac{\Delta z_k}{2}}^{z_k+\frac{\Delta z_k}{2}} z^{\alpha_z r} dz\right), \tag{5.16}$$

where

$$m_{pqr}^{\alpha_x\alpha_y\alpha_z} = \frac{1}{(\alpha_x p+1)(\alpha_y q+1)(\alpha_z r+1)}\left[u_{i+1}^{\alpha_x p+1} - u_i^{\alpha_x p+1}\right]\left[v_{j+1}^{\alpha_y q+1} - v_j^{\alpha_y q+1}\right] \left[w_{k+1}^{\alpha_z r+1} - w_k^{\alpha_z r+1}\right], \tag{5.17}$$

with

$$\begin{array}{l} \mathrm{u}_i = (i-0.5)\,\Delta x_i \;;\; v_j = (j-0.5)\,\Delta y_j \;;\; w_k = (k-0.5)\,\Delta z_k \\ u_{i+1} = (i+0.5)\,\Delta x_i \;;\; v_{j+1} = (j+0.5)\,\Delta y_j \;;\; w_{k+1} = (k+0.5)\,\Delta z_k. \end{array} \tag{5.18}$$

We can define the centroids of the *x*-, *y*-, and *z*-coordinates, respectively $\tilde{x}, \tilde{y}$ and $\tilde{z}$ by:

$$\tilde{x} = \frac{FrGM_{100}^{\alpha_x\alpha_y\alpha_z}}{FrGM_{000}^{\alpha_x\alpha_y\alpha_z}} \;,\; \tilde{y} = \frac{FrGM_{010}^{\alpha_x\alpha_y\alpha_z}}{FrGM_{000}^{\alpha_x\alpha_y\alpha_z}} \;,\; \tilde{z} = \frac{FrGM_{001}^{\alpha_x\alpha_y\alpha_z}}{FrGM_{000}^{\alpha_x\alpha_y\alpha_z}} \tag{5.19}$$

The above definition Eq.(5.14) is given for image coordinates x_i, y_j and z_k with positive values. To avoid problem that the expressions $x_i^{\alpha_x p}, y_j^{\alpha_y q}$ or $z_k^{\alpha_z r}$ may be undefined for $x_i, y_j, z_k < 0$, we assume that α_x, α_y and α_z have an odd denominator and can be written as $\frac{a}{2b+1}$ with $a, b \in \mathrm{N}$ where $a \neq 0$. The fractional-order central moments which are translation invariants are:

$$\eta_{pqr}^{\alpha_x\alpha_y\alpha_z} = \sum_{i=0}^{N-1}\sum_{j=0}^{M-1}\sum_{k=0}^{K-1} f(i,j,k)\, T_{pqr}^{\alpha_x\alpha_y\alpha_z}(x_i,y_j,z_k), \tag{5.20}$$

where

$$T_{pqr}^{\alpha_x\alpha_y\alpha_z} = \int_{x_i-\frac{\Delta x_i}{2}}^{x_i+\frac{\Delta x_i}{2}} \int_{y_i-\frac{\Delta y_j}{2}}^{y_i+\frac{\Delta y_j}{2}} \int_{z_k-\frac{\Delta z_k}{2}}^{z_k+\frac{\Delta z_k}{2}} (x-\hat{x})^{\alpha_x p} (y-\hat{y})^{\alpha_y q} (z-\hat{z})^{\alpha_z r} \, dxdydz. \tag{5.21}$$

with $\alpha_x, \alpha_y \text{ and } \alpha_z$ must satisfy the condition that they have an odd denominator.

Then, by applying the separability property of the moments of the principal function, we can write the triple integral in Eq.(5.21) as follows:

$$\begin{aligned} T_{pqr}^{\alpha_x\alpha_y\alpha_z} = \frac{1}{(\alpha_x p+1)(\alpha_y q+1)(\alpha_z r+1)} & \left[(u_{i+1}-\hat{x})^{\alpha_x p+1} - (u_i-\hat{x})^{\alpha_x p+1}\right] \\ & \times \left[(v_{j+1}-\hat{y})^{\alpha_y q+1} - (v_j-\hat{y})^{\alpha_y q+1}\right] \\ & \left[(w_{k+1}-\hat{z})^{\alpha_z r+1} - (w_k-\hat{z})^{\alpha_z r+1}\right]. \end{aligned} \tag{5.22}$$

In this section we consider the Euler Angle Sequence (θ, φ, ψ), which is commonly used in aerospace engineering and computer graphics. First rotate θ angle along x-axis, next, rotate φ angle along y-axis and finally rotate ψ along z-axis [13, 4]. In general, the 3D rotation matrix can be considered as a linear transformation of the 3D object coordinates, as follows:

$$\begin{pmatrix} x' \\ y' \\ z' \end{pmatrix} = R_{xyz}(\theta,\phi,\psi) \begin{pmatrix} x-\hat{x} \\ y-\hat{y} \\ z-\hat{z} \end{pmatrix} = \begin{pmatrix} \mathrm{R}_{11} & \mathrm{R}_{12} & \mathrm{R}_{13} \\ \mathrm{R}_{21} & \mathrm{R}_{22} & \mathrm{R}_{23} \\ \mathrm{R}_{31} & \mathrm{R}_{32} & \mathrm{R}_{33} \end{pmatrix} \begin{pmatrix} x-\hat{x} \\ y-\hat{y} \\ z-\hat{z} \end{pmatrix} \tag{5.23}$$

with (R_{ij}) $\begin{matrix} 1 \le \mathrm{i} \le m \\ 1 \le \mathrm{j} \le n \end{matrix}$ are the elements of $R_{xyz}(\theta,\phi,\psi)$ matrix.

The 3D geometric moment invariants of fractional order (FrGMIs), $FGMI_{pqr}^{\alpha_x\alpha_y\alpha_z}$, which are independent of rotation, scaling and translation transforms, are:

$$FrGMI_{pqr}^{\alpha_x\alpha_y\alpha_z} = \lambda^{-\gamma} \sum_{i=0}^{N-1} \sum_{j=0}^{M-1} \sum_{k=0}^{K-1} f(i,j,k) \mu_{pqr}^{\alpha_x\alpha_y\alpha_z}(x_i, y_j, z_k) \tag{5.24}$$

where

$$\begin{aligned} \mu_{pqr}^{\alpha_x\alpha_y\alpha_z} = \int_{x_i-\frac{\Delta x_i}{2}}^{x_i+\frac{\Delta x_i}{2}} \int_{y_i-\frac{\Delta y_j}{2}}^{y_i+\frac{\Delta y_j}{2}} \int_{z_k-\frac{\Delta z_k}{2}}^{z_k+\frac{\Delta z_k}{2}} & \Big[\\ & (\mathrm{R}_{11}(x-\hat{x}) + \mathrm{R}_{12}(y-\hat{y}) + \mathrm{R}_{13}(z-\hat{z}))^{\alpha_x p} \\ & (\mathrm{R}_{21}(x-\hat{x}) + \mathrm{R}_{22}(y-\hat{y}) + \mathrm{R}_{23}(z-\hat{z}))^{\alpha_y q} \\ & (\mathrm{R}_{31}(x-\hat{x}) + \mathrm{R}_{32}(y-\hat{y}) + \mathrm{R}_{33}(z-\hat{z}))^{\alpha_z r} \end{aligned} \, dxdydz. \tag{5.25}$$

The normalization parameters $\gamma, \lambda, \theta, \varphi$ and ψ the rotational invariants can be obtained by normalizing the transformed 3D object, are defined in [4]. For $\alpha_x+\alpha_y+\alpha_z = 1$, they can be determined as follows:

$$\lambda = FrGM_{000}^{\alpha_x\alpha_y\alpha_z} \ , \ \gamma = 1 + \frac{\alpha_x n + \alpha_y m + \alpha_z p}{3}$$
$$\theta = \frac{1}{2}\tan^{-1}\left(\frac{2\eta_{011}}{\eta_{020}+\eta_{002}}\right) \ , \ \varphi = \frac{1}{2}\tan^{-1}\left(\frac{2\eta_{101}}{\eta_{200}+\eta_{002}}\right) \ , \ \psi = \frac{1}{2}\tan^{-1}\left(\frac{2\eta_{110}}{\eta_{200}+\eta_{020}}\right). \tag{5.26}$$

The exact calculation of this integral Eq.(5.25) is very difficult or even impossible. We refer the readers to [6] for analytic computation of the triple integrals $m_{pqr}^{\alpha_x\alpha_y\alpha_z}$ and $T_{pqr}^{\alpha_x\alpha_y\alpha_z}$, based on their separability property. While, for the integral $\mu_{pqr}^{\alpha_x\alpha_y\alpha_z}$ of Eq.(5.25), we suggest the use of numerical integration technique, for instance Simpson's rule or Gaussian quadrature [47], since it is difficult to split the triple integral of Eq.(5.25) into three simple 1-D integrals.

5.3.2 FrLM Invariants

This subsection aims to present the efficiency the computation of Fractional-order Legendre Moment Invariants (FrLMIs) for any of their parameters values, with respect to transformations, RST. We define FrLMs for a given weighted image intensity function $\tilde{f}(i,j,k) = \left[w_{\alpha_x}(x)w_{\alpha_y}(y)w_{\alpha_z}(z)\right]^{-1/2} f(i,j,k)$, of size $N \times M \times K$ voxels, with $w_\alpha(x)$ is the weight function of FrLPs, as follows:

$$\begin{aligned} FrLM_{nmp}^{\alpha} &= \int_0^1\int_0^1\int_0^1 \tilde{f}(i,j,k)\widetilde{FrL}_n^{\alpha_x}(x_i)\widetilde{FrL}_m^{\alpha_y}(y_j)\widetilde{FrL}_p^{\alpha_z}(z_k)dxdydz \\ &= \frac{1}{\sqrt{d_{n,\alpha_x}^2 d_{m,\alpha_y}^2 d_{p,\alpha_z}^2}} \int_0^1\int_0^1\int_0^1 f(i,j,k)FrL_n^{\alpha_x}(x_i)FrL_m^{\alpha_y}(y_j)FrL_p^{\alpha_z}(z_k)dxdydz \end{aligned} \tag{5.27}$$

By the help of Eq.(5.12) and Eq.(5.8), we can express the FrLMs in terms of the Fractional-order Geometric Moments $FrGM_{pqr}^{\alpha_x\alpha_y\alpha_z}$, based on the relation between $FrL_n^\alpha(t)$ and the polynomials of $t^{\alpha k}$:

$$FrLM_{nmp}^{\alpha} = \frac{1}{\sqrt{d_{n,\alpha_x}^2 d_{m,\alpha_y}^2 d_{p,\alpha_z}^2}} \sum_{l=0}^{n}\sum_{s=0}^{m}\sum_{r=0}^{p} B_{n,l}B_{m,s}B_{p,r}FrGM_{lsr}^{\alpha_x\alpha_y\alpha_z}. \tag{5.28}$$

In order to obtain the invariants of rotation, scaling and translation of FrLMs, which will be denoted by $FrLMI_{nmp}^{\alpha}$ along this paper, the terms $FrGM_{pqr}^{\alpha_x\alpha_y\alpha_z}$ in the previous equation will be replaced by the $FrGMI_{pqr}^{\alpha_x\alpha_y\alpha_z}$ of Eq.(5.24):

$$FrLMI_{nmp}^{\alpha} = \frac{1}{\sqrt{d_{n,\alpha_x}^2 d_{m,\alpha_y}^2 d_{p,\alpha_z}^2}} \sum_{l=0}^{n}\sum_{s=0}^{m}\sum_{r=0}^{p} B_{n,l}B_{m,s}B_{p,r}FrGMI_{lsr}^{\alpha_x\alpha_y\alpha_z} \tag{5.29}$$

The direct computation of the coefficients $B_{n,k}$ defined in Eq.(5.8) involves the evaluation of factorial terms for each value of n and k. Based on the property that $n! = n\,(n-1)!$, the coefficients $B_{n,k}$ of Eq.(5.8) can be easily computed using the following recursive method:

$$B_{n,k} = -\frac{(n+k)(n-k+1)}{k^2}\, B_{n,k-1} \text{ for } 1 \leq k \leq n, \text{ and } B_{n,0} = (-1)^n \quad (5.30)$$

It is clearly seen from Eq.(5.30) that the recursive method is free from factorial terms and it is more adequate for the computation of the polynomial coefficients $B_{n,k}$, which could considerably reduce the time required for computing moment invariants, also for enhancing their numerical stability, since it is free from factorial terms [39, 40].

5.4 Fractional-order Discrete Orthogonal Moments (FrDOMs)

Discrete orthogonal moments have been carefully studied due to their peculiarity of being directly defined in the discrete image/signal domain, as their kernel consists of discrete orthogonal polynomials and, therefore, they are suitable for digital images. An overview of discrete orthogonal polynomials such as de Tchebichef, Krawtchouk, Hahn, Charlier and Meixner and their corresponding moments can be found in reference [60]. All discrete orthogonal moments based on the discrete orthogonal polynomials mentioned above are limited to be of integer order since the basic discrete orthogonal polynomials are of integer order.

Recently, the focus has been on the study of discrete orthogonal polynomials of fractional order which are used as kernel functions to define discrete orthogonal moments of fractional order (FrDOMs) such as fractional-order Krawtchouk moments [35], fractional-order Tchebichef moments [51] and fractional-order Charlier moments [53]. The classical versions of integer order (DOMs) are special cases of FrDOMs. These fractional-order descriptors are successfully used in different image processing fields such as image watermarking, image reconstruction and image encryption.

In the following, we discuss in detail the properties of fractional-order discrete orthogonal polynomials and their corresponding moments. Due to the limited paper length, we present the mathematical context of fractional-order Charlier moments [53], including the algebraic expansion and the properties of the eigenvalues and eigenvectors of the kernel function.

We start with the classical Charlier polynomials of integer order, then we present the fractional-order version of the Charlier polynomials and finally we give their corresponding moments.

5.4.1 Classical Charlier polynomials

The Charlier polynomials satisfy the following orthogonal condition [60],

$$\sum_{x=0}^{\infty} \omega_C(x) c_n^{a_1}(x) c_m^{a_1}(x) = \rho_C(n)\delta_{nm} \;\; ; \quad n, m \geq 0 \quad (5.31)$$

where $\rho_C(n) = n!/{a_1}^n$, $\omega_C(x) = e^{-a_1}{a_1}^x/x!$ and the Charlier polynomials $c_n^{a_1}(x)$ are defined as

$$c_n^{a_1}(x) = {}_2F_0(-n, -x; -\frac{1}{a_1}), \quad n, x = 0, 1, 2.....\infty \tag{5.32}$$

where $a_1 \in \mathrm{R}^+$ and ${}_2F_0()$ is the generalized hypergeometric function given by:

$${}_2F_0(a, b; \ ; c) = \sum_{k=0}^{n} \frac{(a)_k (b)_k (c)^k}{k!} \tag{5.33}$$

and $(a)_k = a(a+1)(a+2)...(a+k-1)$ denotes the pochhammer symbol.
The normalized Charlier polynomial $\tilde{c}_n^{a_1}(x)$ was defined by *Zhu et al.* [60] as

$$\tilde{c}_n^{a_1}(x) = c_n^{a_1}(x) \sqrt{\frac{\omega_C(x)}{\rho_C(n)}} \tag{5.34}$$

The relation of orthogonality changes to

$$\sum_{x=0}^{\infty} \tilde{c}_n^{a_1}(x) \tilde{c}_m^{a_1}(x) = \delta_{n,m}, \quad n, m \geq 0 \tag{5.35}$$

The Charlier polynomials satisfy a three-term recurrence relation of type

$$\tilde{c}_n^{a_1}(x) = A \tilde{c}_{n-1}^{a_1}(x) + B \tilde{c}_{n-2}^{a_1}(x) \tag{5.36}$$

where

$$A = \frac{-x + n - 1 + a_1}{a_1} \sqrt{\frac{a_1}{n}}, \qquad B = \frac{1 - n}{a_1} \sqrt{\frac{{a_1}^2}{n(n-1)}} \tag{5.37}$$

with the initial conditions

$$\tilde{c}_0^{a_1}(x) = \sqrt{\frac{\omega_C(x)}{\rho_C(0)}}, \qquad \tilde{c}_0^{a_1}(x) = \frac{a_1 - x}{a_1} \sqrt{\frac{\omega_C(x)}{\rho_C(1)}} \tag{5.38}$$

5.4.2 Fractional-order Charlier Polynomials (FrCPs)

According to the Eqs. (5.31) and (5.35), the Charlier polynomials $\tilde{c}_n^{a_1}(x)$ are orthogonal over the interval $[0, \infty[$. To implement these polynomials in a finite interval $[0, N]$, *Yamni et al.* In [53] recommended to use the Gram-Schmidt Process (GSP) to solve this truncation problem in order to make these polynomials orthogonal in this finite interval. Therefore, the Charlier polynomials modified by GSP $\hat{c}_n^{a_1}(x)$ are orthogonal to the interval $[0, N]$.

The discrete Charlier polynomial matrix $\hat{C}$ of size N is defined by

$$\hat{C}_{n,x} = \hat{c}_n^{a_1}(x), \ \ 0 \leq n, x \leq N - 1. \tag{5.39}$$

The eigenvalues of $\hat{C}$ are $\lambda_1 = 1$ and $\lambda_2 = -1$ and their multiplicities are shown in Table 5.1 [53].

Table 5.1: Multiplicities of the eigenvalues for matrix $\hat{C}$.

N	Multiplicity of $\lambda_1 = 1$	Multiplicity of $\lambda_2 = -1$
Even	$N/2$	$N/2$
Odd	$(N+1)/2$	$(N-1)/2$

$\hat{C}$ is a symmetric and orthogonal real matrix. According to the spectral theorem [15], $\hat{C}$ has the following spectral decomposition:

$$\hat{C} = \sum_{k=1}^{2} \lambda_k P_k = \lambda_1 P_1 + \lambda_2 P_2 \tag{5.40}$$

where $\boldsymbol{P}_i,\ i = 1, 2$, is the orthogonal projection matrix on the *i*th eigenspace of $\hat{C}$. The two projection matrices of $\hat{C}$ (P_1 and P_2) can be derived as follows [53]:

$$P_1 = 0.5(I + \hat{C}), \qquad \mathrm{P}_2 = 0.5(I - \hat{C}) \tag{5.41}$$

The method of deriving the two projection matrices P_1 and P_2 is presented in detail in [53].

P_1 and P_2 satisfy the following properties:

a. $P_i^T = P_i,\ i = 1, 2.$

b. $P_i^2 = P_i,\ i = 1, 2.$

c. $P_1 P_2 = 0$, where 0 denotes the zero matrix.

d. Both matrices P_1 and P_2 have eigenvalues 0 and 1.

e. The multiplicity of eigenvalue 1 for P_1 is equal to the multiplicity of eigenvalue 1 of $\hat{C}$; the multiplicity of eigenvalue 1 for P_2 is equal to the multiplicity of eigenvalue -1 of $\hat{C}$.

f. The eigenvectors corresponding to nonzero eigenvalues of P_1 are orthogonal to those corresponding to nonzero eigenvalues of P_2.

g. The eigenvectors corresponding to nonzero eigenvalues of P_1 and P_2 are the eigenvectors of $\hat{C}$, corresponding to eigenvalues λ_1, λ_2 of $\hat{C}$, respectively.

h. The multiplicity of the eigenvalue 1 for P_1 and P_2 is both $N/2$ if N is even, and if N is odd, the multiplicity of eigenvalue 1 for P_1 is $(N+1)/2$, and the multiplicity of eigenvalue 1 for P_2 is $(N-1)/2$.

To derive an orthonormal basis for each orthogonal projection matrix P_i, *Yamni et al.* applied the singular-value decomposition technique. The singular-value decomposition of P_1 and P_2 is

$$P_1 = U_1 S_1 V_1^T, \qquad \mathrm{P}_2 = U_2 S_2 V_2^T \tag{5.42}$$

where $U_i$and V_i are unitary matrices of order N and matrix S_i contains in its diagonal coefficients the singular values of the matrix P_i.

$V_1$and V_2 are a set of orthonormal eigenvectors of P_1 and P_2, respectively, because they check the following condition [53]:

$$P_1 V_1 = \mathbf{V}_1 \mathbf{S}_1, \qquad \mathbf{P}_2 \mathbf{V}_2 = \mathbf{V}_2 \mathbf{S}_2 \tag{5.43}$$

A set of orthonormal eigenvectors $V$of $\hat{C}$ can be obtained from $V_1$and V_2 as follows:

$$V = \begin{cases} [u_1, u_2, ..., u_{\frac{N}{2}}, v_1, v_2, ..., v_{\frac{N}{2}}] \,, & \text{if } N \text{ is even} \\ [u_1, u_2, ..., u_{\frac{N-1}{2}}, u_{\frac{N+1}{2}}, v_1, v_2, ..., v_{\frac{N-1}{2}}], & \text{if } N \text{ is odd} \end{cases} \tag{5.44}$$

where u_i and v_j are the i^{th} and j^{th} column of $V_1$and V_2.

The columns of V can be rearranged to match the eigenvectors to the eigenvalues of $\hat{C}$ such that

$$\hat{C} = \hat{V} D \hat{V}^T \tag{5.45}$$

where D is a diagonal matrix with diagonal entries the eigenvalues of $\hat{C}$, which are arranged in the following form

$$D = \begin{cases} Diag\{1, -1, 1, ..., -1\}, & \text{if } N \text{ is even} \\ Diag\{1, -1, 1, ..., -1, 1\}, & \text{if } N \text{ is odd} \end{cases} \tag{5.46}$$

and $\hat{V}$ is a set of orthonormal eigenvectors

$$\hat{V} = \begin{cases} [u_1, v_1, u_2, v_2....., u_{\frac{N}{2}}, v_{\frac{N}{2}}], & \text{if } N \text{ is even} \\ [u_1, v_1, u_2, v_2....., u_{\frac{N-1}{2}}, v_{\frac{N-1}{2}}, u_{\frac{N+1}{2}}], & \text{if } N \text{ is odd} \end{cases} \tag{5.47}$$

To define the fractional-order Charlier polynomials(FrCPs), *Yamni et al.* [53] took the fractional order as the power of the diagonal matrix D. The FrCP matrix $\hat{C}^a$ of size N with order $\alpha \in \mathrm{R}$ can be defined as:

$$\hat{C}^{\alpha} = \hat{V} D^{\alpha} \hat{V}^T = \sum_{k=0}^{N-1} e^{-jk\alpha\pi} \hat{v}_k \hat{v}_k^T \tag{5.48}$$

where $\hat{V} = [\hat{v}_0, \hat{v}_1, ..., \hat{v}_{N-1}]$ with $\hat{v}_k$ $(k = 0, 1, ..., N-1)$ is the $\hat{C}$ eigenvector obtained from (Eq. (5.52)), and D^{α} is defined as:

$$D^{\alpha} = Diag\{1, e^{-j\alpha\pi}, e^{-j2\alpha\pi}, ..., e^{-j(N-1)\alpha\pi}\} \tag{5.49}$$

$\hat{C}^{\alpha}$ checks some important properties such as unitary (i.e. $\hat{C}^{-\alpha} = (\hat{C}^{\alpha})^{-1}$), index additivity (i.e. $\hat{C}^{\alpha+\beta} = \hat{C}^{\alpha}\hat{C}^{\beta} = \hat{C}^{\beta+\alpha} = \hat{C}^{\beta}\hat{C}^{\alpha}$), and reduction to the conventional matrix of Charlier polynomials $\hat{C}$ when the order α is equal to 1, and to the identity matrix I when the order α is equal to 0.

5.4.3 Fractional-order Discrete Orthogonal Moments (FrDOMs)

The fractional-order discrete orthogonal moments are a set of moments formed by the fractional discrete polynomials. The 1D FrDOMs with fractional order $\alpha \in \mathrm{R}$ can be expressed by

$$FrM^{\alpha} = FrP^{\alpha} f \tag{5.50}$$

where FrM^{α} are the coefficients in the DFrDOM domain, $f(x)$ is one-dimensional signal with length N, FrP^{α} is a fractional polynomial matrix of size N with order α as the moment basis set.

The 1D FrKMs [35], 1D FrTMs [51], or 1D FrCMs can be obtained if FrP^{α} is set as K^{α}[35], H^{α}[51], or $\hat{C}^{\alpha}$Eq. (5.53), respectively.

The reconstruction of the signal f can be found from its FrDOMs by using the following expression:

$$f = FrP^{-\alpha} FrM^{\alpha} \tag{5.51}$$

In the case of a digital image $f(x, y)$, with size $N \times M$, the 2D FrDOMs with fractional orders $\alpha, \beta \in \mathrm{R}$ can be expressed by

$$FrM^{\alpha,\beta} = FrP_1^{\alpha} f FrP_2^{\beta} \tag{5.52}$$

where FrP_1^{α} is a fractional polynomial matrix of size $N \times N$ with order α, and FrP_2^{β} is a fractional polynomial matrix of size $M \times M$ with order β.

By choosing $(FrP_1^{\alpha} \& FrP_2^{\beta})$ as $(K^{\alpha} \& K^{\beta})$ [35], $(H^{\alpha} \& H^{\beta})$ [51], and $(\hat{C}^{\alpha} \& \hat{C}^{\beta})$, one can obtain the 2D FrKMs [35], 2D FrTMs [51], and 2D FrCMs, respectively.

The previous equation also leads to the following inverse moment transform

$$f = FrP_1^{-\alpha} FrM^{\alpha,\beta} FrP_2^{-\beta} \tag{5.53}$$

5.5 Experiments, Results and Discussion

In this section, several experiments are performed to validate the performance and efficiency of fractional orthogonal moments (FrCOMs and FrDOMs) compared to classical integer-order moments (COMs and DOMs). We first examine the capacity of FrCOMs on 2D/3D image reconstruction. Then, the invariants of FrCOMs are tested in terms of RST invariability and in terms of 2D/3D image recognition. Finally, we show the efficiency of FrDOMs in terms of imperceptibility, robustness and security of the watermarking scheme.

5.5.1 2D and 3D image reconstruction using FrCOMs

2D and 3D Images reconstruction using orthogonal moments is an essential process in different image processing applications. To demonstrate the image representation capability of the introduced FrLMs in comparison with the existing Chebyshev Moments (ChMs) [59], Gegenbauer Moments (GegMs) [20], Generalized Laguerre Moments (GLMs) [34] and Gaussian--Hermite Moments (GHMs) [55], we are conducted

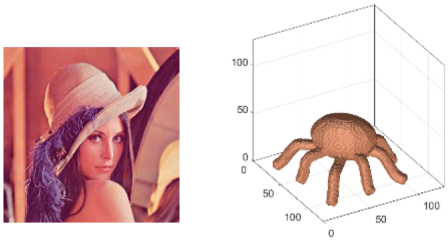

(a) (b)

Figure 5.2: (a) Original Lena test color images.(b) 3D image «Crabs» from PSB database [3].

to use the Mean Squared Error (MSE) to measure the reconstruction error between the original image $f(x, y, z)$ and the reconstructed one $\hat{f}(x, y, z)$. The MSE is defined as:

$$MSE = \frac{1}{NMK} \sum_{x=0}^{N-1} \sum_{y=0}^{M-1} \sum_{z=0}^{K-1} \left[f(x, y, z) - \hat{f}(x, y, z) \right]^2 \tag{5.54}$$

Figure 5.3 and Fig. 5.4 depict a comparison between FrLMs, ChMs, GegMs, GLMs and GHMs, in terms of reconstruction quality of Lena image of size 512×512 and 3D image "Crabs" of size $128 \times 128 \times 128$, which shown in Fig. 5.2. Moreover, we considered different fractional parameters values: (A) $\alpha_x = \alpha_y = \alpha_z = 0.4$, (B) $\alpha_x = 1.2,\ \alpha_y = 1,\ \alpha_z = 1.2$ and (C) $\alpha_x = \alpha_y = \alpha_z = 1.4$. From Fig. 5.3 and Fig. 5.4, one can clearly observe that the quality of the reconstructed image becomes closer to the original one with the increases of moments orders. In addition, the FrLMs show more visual resemblance to the original images in the early orders, noting the absence of reconstruction errors for the higher orders.

To further illustrate the performance of the fractional-order moments, Fig. 5.5(a) and Fig. 5.5(b) show a comparison between the FrLMs, ChMs, GegMs, GLMs and GHMs, in terms of the MSE values of Lena image reconstruction and 3D image «Crabs», for an increasing moments order from 0 to 600 and 0 to 130 respectively. As a result, derived from Fig. 5.5, we can deduce that the FrLMs outperformed all other existing classical methods. These results ensure the accuracy and stability of the FrLMs method.

5.5.2 Invariability property of FrCOMIs

Invariances to RST, are essential characteristics for pattern recognition and computer vision applications. This experiment aims to verify the rotation, scaling and translation in variance of the FrLMIs. We used the «Crabs» test 3D image of size $128 \times 128 \times 128$ pixels, which is selected from Princeton Shape Benchmark (PSB) database [3] and shown in Fig. 5.2. The test image is firstly translated by vector varying from

Figure 5.3: The reconstruction color images Lena, using FrLMs, ChMs, GegMs and GLMs for different values of the maximum moment order n, m = 50, 150, 300, 500, 600.

$(-15,-15,-15)$ to $(15,15,15)$ with step $(2,2,2)$. Then, scaled by factors starting from 0.4 to 1.4 with interval 0.05 and finally rotated by a rotation angle varying between 0° and 360° with interval 10°. Then, the moment invariants coefficients of each transformed image are computed up to the third order $(n+m\leq 3)$ using four cases: (A) $\alpha_x = \alpha_y = \alpha_z = 1.4$, (B) $\alpha_x = 1.4$, $\alpha_y = 1$, $\alpha_z = 0.4$ and (C) $\alpha_x = \alpha_y = \alpha_z = 0.4$. Subsequently, the relative error between moment invariants coefficients of the original image and the transformed one is computed, as follows:

$$\mathrm{RE}\left(f, f^d\right) = \frac{\left\|FrLMI(f) - FrLMI(f^d)\right\|}{\|FrLMI(f)\|} \tag{5.55}$$

where $\|\|$, f, and f^d designate the Euclidean norm, the original images and the deformed images, respectively. It should be emphasized that a very small relative error leads to a good invariance.

The corresponding results for scale and rotation invariance are illustrated respectively in Fig. 5.6(a) and Fig. 5.6(b). While the results for translation invariance are not included, since the values of FrLMIs for all translation vectors remain unchangeable, which lead to a relative error equals to zero. Furthermore, to understand the effect of noise on the FrLMIs moment invariants, the test image has been corrupted by different kind of noise. First, distorted by different densities of Salt-and-Pepper noise varying from 0% to 5% with interval 0.25%. Second, distorted by Gaussian noise with zero mean and standard deviation varying from 0 to 0.5 with step 0.05. Figure 5.6(c) and Fig. 5.6(d) depict respectively the robustness of FrLMIs against Salt-and-Pepper and Gaussian noise.

Again, the FrLMIs show small relative errors values which ensure the highly accurate invariances to the RST geometric transformations. Moreover, they express high

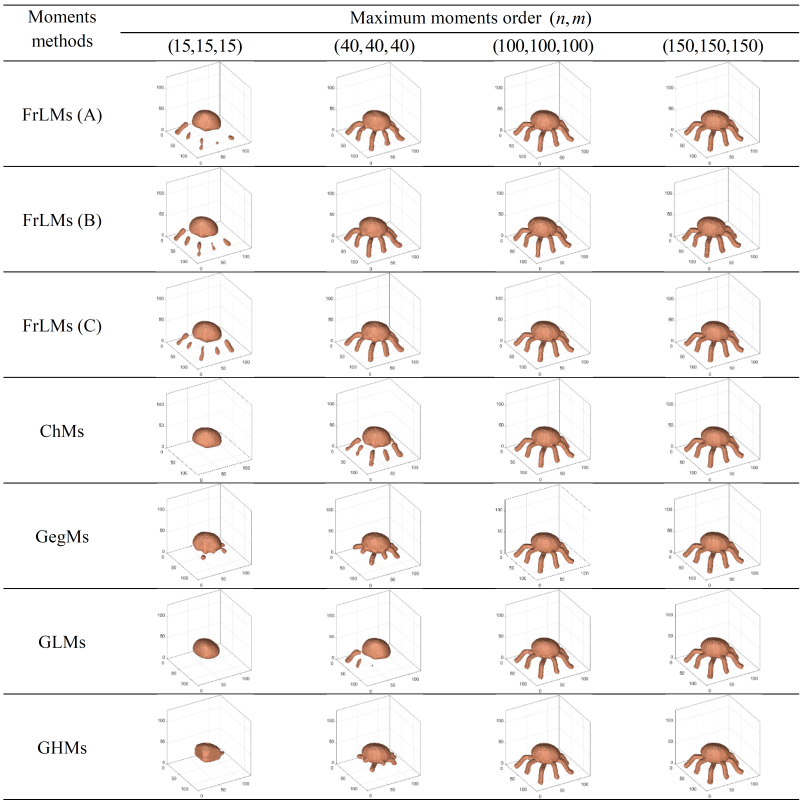

Figure 5.4: 3D image «Crabs» reconstruction results, using FrLMs, ChMs, GegMs, GLMs and GHMs for different values of the maximum moment order n, m, p = 15, 40, 100, 130.

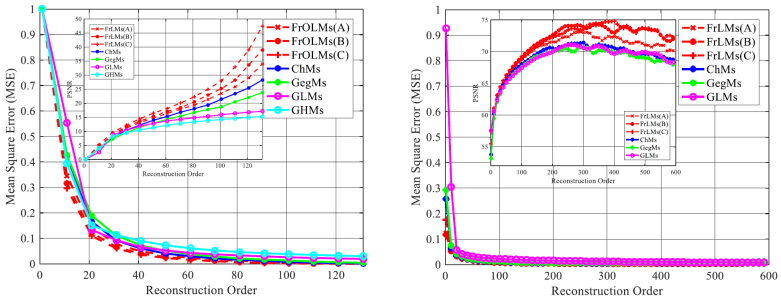

(a) (b)

Figure 5.5: Comparative study of image reconstruction error of the FrLMs and the existing classical orthogonal moments [59, 20, 34, 55]. (a) 3D image «Crabs» (b) Lena color image.

tolerance against different kinds of noise. These new fractional-order moments outperformed the existing integer-order orthogonal moments . Eventually, this new set of invariants could provide an efficient and stable feature representation for image classification problems.

5.5.3 Classification of 2D and 3D images using FrCOMIs

In this subsection, the recognition ability of the FrLMIs moment invariants in both noise free and noisy conditions is evaluated using the well-known databases are adopted: Princeton Shape Benchmark (PSB) [3] and COIL-100 [1]. Basically, this experiment is conducted on two testing sets, which have been created by selecting 20 images of different classes from each database, which are shown in Fig. 5.7(a) and Fig. 5.7(b). The size of the images is unified to be 128×128 pixel, and $128\times128\times128$ voxels for 3D images. Each image in these testing sets is affected by a series of transforms (8 rotation $+8$ translations $+8$ scaling $+8$ mixed transforms), in order to generate 640 images per database. Furthermore, to assess the noise robustness of moment invariants, five additional testing databases are created by adding different densities of Salt-and-Pepper noise $\{1\%; 2\%; 3\%; 4\%; 5\%\}$.

The 2D and 3D image classification performance of FrOLMIs is compared with the existing methods, Chebyshev Moment invariants (ChMIs) [59], Gegenbauer Moment invariants (GegMIs) [20], Generalized Laguerre Moment invariants (GLMIs) [34], Gaussian--Hermite Moment invariants (GHMIs) [55] and the well-known moment invariants GMI [48], using the 1-NN (k- Nearest Neighbors with $k = 1$) classifier with 5-folds cross validation and moment invariants up to order 5 are considered. Finally, we have considered three testing cases of FrOLMIs: (A) $\alpha_x = \alpha_y = \alpha_z = 1.4$, (B) $\alpha_x = 1.4$, $\alpha_y = 1$, $\alpha_z = 0.4$, (C) $\alpha_x = 0.4$, $\alpha_y = 1.4$, $\alpha_z = 1$ and (D) $\alpha_x = \alpha_y = \alpha_z = 0.4$. The obtained classification results are listed in Table 2. This table shows that the FrLMIs outperformed the existing classical methods ChMIs [59], GegMIs [20], GLMIs [34], GHMIs [55] and GMI [48] in terms of classification accuracy.

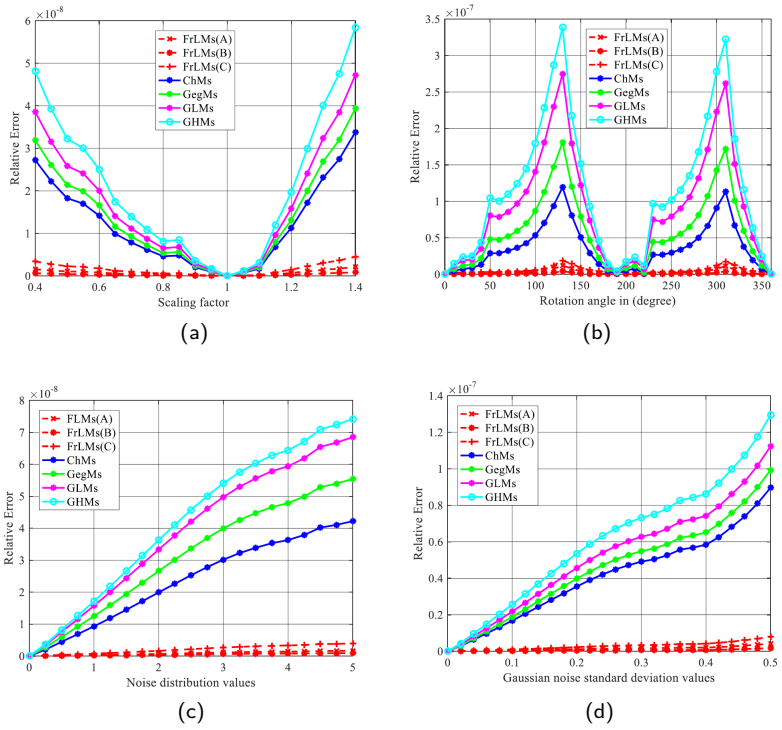

Figure 5.6: Relative error of the FrLMIs using 3D image « Crabs » by: scaling transformation (a), rotation (b), Salt-and-Pepper noise (c) and Gaussian noise (d).

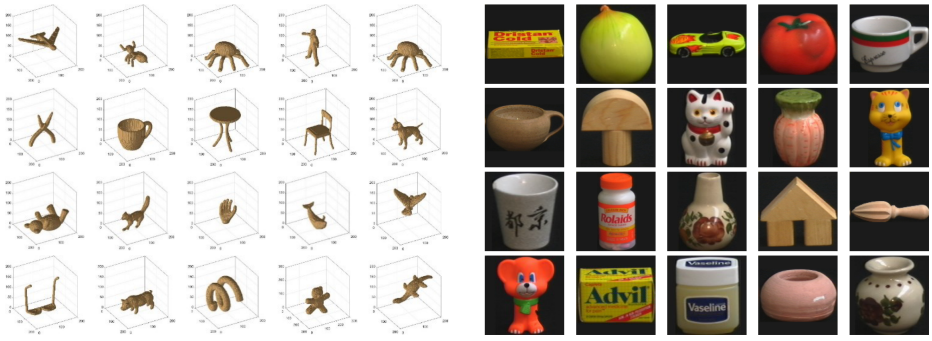

Figure 5.7: The selected images from each database: , (a) PSB [3] and (b) Coil-100 [1].

Table 5.2: Classification accuracy (%) of PSB [3] and Coil-100 [1] database, by using FrLMIs, ChMIs, GegMI, GLMIs, GHMIs and GMI.

Database		PSB [3]							Coil-100 [1]					
Moments invari-ants	Noise-Free	Salt and Pepper noise					**Average**	Noise-free	Salt and Pepper noise					**Average**
		1%	2%	3%	4%	5%			1%	2%	3%	4%	5%	
FrLMIs (A)	**99.98**	72.46	**69.57**	59.98	**49.79**	**40.68**	65.410	**100.00**	**76.58**	70.42	**61.84**	55.26	**53.84**	**69.657**
FrLMIs (B)	**99.72**	72.24	68.81	59.89	49.53	39.74	64.988	**100.00**	75.98	**70.81**	60.35	54.15	52.77	69.010
FrLMIs (C)	**99.97**	**73.54**	68.94	**60.53**	49.34	40.61	**65.488**	**100.00**	76.41	70.28	61.64	**55.72**	53.75	69.633
FrLMIs (D)	**99.61**	71.72	68.52	59.68	48.18	39.14	64.475	**99.93**	74.97	69.53	60.18	53.38	51.78	68.295
ChMIs [59]	97.38	68.62	60.16	51.93	40.14	30.93	58.193	99.28	73.28	69.24	60.21	50.42	49.15	66.930
GegMIs [20]	96.94	69.32	59.95	50.28	39.32	30.87	57.780	99.04	72.42	68.65	59.84	48.68	49.86	66.415
GLMIs [34]	94.89	65.79	57.92	53.50	35.96	29.78	56.307	99.41	72.78	68.74	59.45	49.24	48.23	66.308
GHMIs [55]	92.55	59.56	56.29	52.40	34.44	26.27	53.585	98.95	73.24	67.24	59.67	48.29	47.17	65.760
GMIs [48]	75.65	53.23	36.37	30.88	21.73	14.57	38.738	97.87	50.21	45.73	34.53	27.77	29.25	47.560

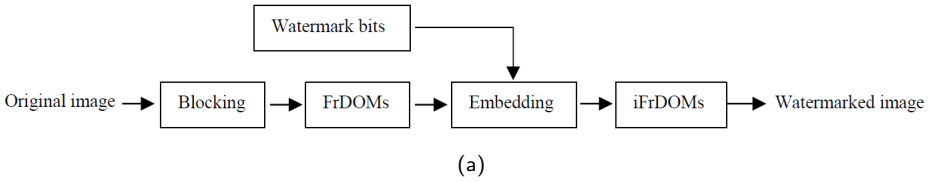

Figure 5.8: Watermark embedding.

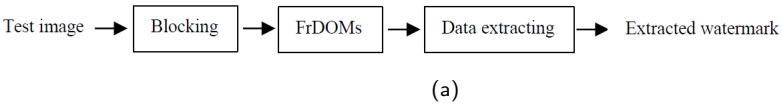

Figure 5.9: Watermark extraction.

5.5.4 Watermarking based on the FrDOMs

The authors in [35], [51] and [53] proposed image watermarking schemes to verify the performance of FrKMs, FrTMs and FrCMs, respectively, in terms of image copyright protection. In these papers, FrDOM coefficients are used to embed the watermark (hidden information) into the host images. By adjusting the fractional orders of FrDOMs, different transformation domain coefficients can be obtained. In addition, the fractional orders can serve as secret keys to enhance the security of the watermarking scheme.

The main idea of these schemes is to divide the original image into image blocks and then to embed one watermark bit into the FrDOM coefficients of each block by using the Dither modulation, which is a special form of quantization index modulation (QIM) (refer to [35] for more details). After substituting the original FrDOM coefficients by the modified FrDOM coefficients, inverse FrDOMs (iFrDOMs) are performed, and then the watermarked digital image is obtained. The embedding model is shown in Fig. 5.8.

In data extraction, the FrDOMs of test image, which can be a distorted version of the original host image, are calculated in the same way as in the embedding. Then, the watermark bits are extracted using the FrDOM coefficients, the same quantization method and a minimum distance decoder (refer to [35] for more details). The extracting model is shown in Fig. 5.9.

The test materials in the following experiments comprised 96 gray images of size 512×512 from the image database of the Computer Vision Group, University of Granada [2]. A 64×64 binary image is used as watermark to embed in the host image in our experiments.

In this study, the fractional orders in the FrKMs-, FrTMs-, FrCMs-based image watermarking schemes are $(\alpha = 0.4\&\beta = 0.4)$, $(\alpha = 0.9\&\beta = 1.2)$ and $(\alpha = 0.3\&\beta = 0.3)$ as recommended in articles [35], [51] and [53], respectively. Besides, the classical DOMs (KMs, TMs and CMs) of the integer orders $(\alpha = \beta = 1)$ are also considered in the experiments to verify the importance of the fractional versions for

Table 5.3: Average PSNRs resulting from examined watermark schemes.

Watermarking schemes	Average PSNR (dB)
FrKMs	**43.55**
KMs	36.78
FrTMs	**40.37**
TMs	35.29
FrCMs	**45.13**
CMs	32.37

digital image watermarking tasks.

The performance of the algorithm based on FrDOMs is evaluated in terms of imperceptibility using the Peak Signal-to-Noise Ratio (PSNR) as defined as in Eq.(5.56) and in terms of robustness using the Bit Error Rate (BER) defined as defined as in Eq.(5.57):

$$PSNR(dB) = 10\log_{10}\frac{255^2 \times N \times M}{\sum_{x=1}^{N-1}\sum_{y=1}^{M-1}(f(x,y) - \hat{f}(x,y))^2} \tag{5.56}$$

$$BER = \frac{B_{ERR}}{B_T} \tag{5.57}$$

where $\hat{f}$ is the watermarked image, f is the original image, $N \times M$ is the image size, B_{ERR} is the number of erroneous bits and B_T is the total number of watermark bits.

Typically, a larger quantization value Δ (embedding strength of the watermark bit) will demonstrate better robustness in the image watermarking scheme, while the imperceptibility of the watermarked image is reduced. To ensure the watermark's imperceptibility, the PSNR value should be higher than 40 dB. Therefore, in the following experiments, the quantization values Δ are set at 45, 40 and 60 for the schemes based on FrKMs [35], FrTMs [51] and FrCMs [53], respectively.

From the comparison results in Table 5.3, it is clearly shown that for the same quantization value, the average PSNR of the FrDOMs-based watermarking scheme is higher than that of DOMs-based.

In order to illustrate the robust nature of the FrDOMs-based watermarking scheme, attacks including image compression, noise, and image filtering are used to estimate the robustness of the watermarking scheme. Table 5.4 summarizes the comparisons between our proposed watermark extraction results and the results of classical DOMs-based schemes against various attacks. We observe that the FrDOMs-based method obtained a higher watermarking robustness than the classical DOMs-based method in all attack conditions. It can be concluded that the FrDOM-based image watermarking method not only demonstrated good watermark imperceptibility, but also strong watermark robustness.

Table 5.4: Average BER values of the FrDOMs and DOMs based watermarking schemes under different attacks.

Attack type	**FrKMs**	KMs	**FrTMs**	TMs	**FrCMs**	CMs
JPEG compression (70)	**0.0128**	0.0194	**0.0132**	0.0180	**0.0122**	0.0196
JPEG compression (30)	**0.0521**	0.1069	**0.0610**	0.1107	**0.0425**	0.1187
Gaussian noise (0.01)	**0.3015**	0.3200	**0.2810**	0.3402	**0.2760**	0.3300
Gaussian noise (0.03)	**0.3240**	0.3905	**0.3205**	0.4105	**0.3052**	0.4205
Salt & peppers noise (0.01)	**0.0615**	0.1800	**0.0602**	0.1900	**0.0587**	0.2100
Salt & peppers noise (0.03)	**0.1740**	0.2850	**0.1705**	0.2908	**0.1620**	0.2905
Median filtering (3×3)	**0.0591**	0.1695	**0.0652**	0.1840	**0.0360**	0.1803
Median filtering (7×7)	**0.0940**	0.2705	**0.1105**	0.3052	**0.0885**	0.3052
Average filtering (3×3)	**0.0291**	0.2048	**0.0401**	0.1950	**0.0272**	0.1902
Average filtering (7×7)	**0.0840**	0.2705	**0.1105**	0.2727	**0.0885**	0.2952
Gaussian blur (0.5)	**0.0913**	0.1815	**0.0901**	0.1915	**0.0722**	0.1950
Gaussian blur (1)	**0.1940**	0.2652	**0.1805**	0.2505	**0.1125**	0.2605

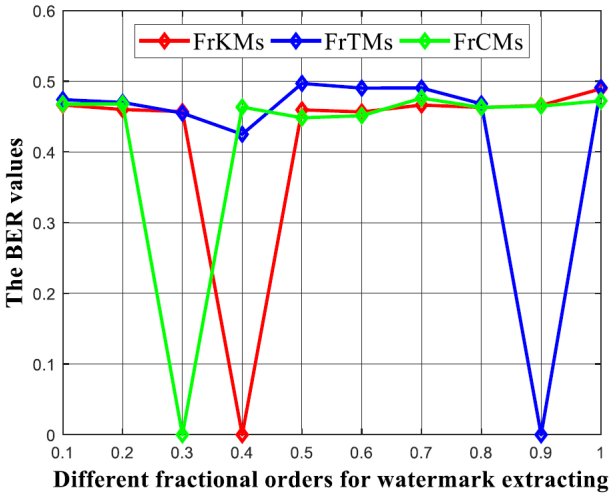

Figure 5.10: BER value of extracted watermark with fractional orders different from the embedding stage in the extraction procedure (with $\alpha = \beta = 0.4$, $\alpha = \beta = 0.9$ and $\alpha = \beta = 0.3$ in the embedding procedure for FrKMs, FrTMs and FrCMs, respectively).

Fractional orders $(a\&b)$ of FrDOMs can be considered as cipher keys in the watermarking scheme, which can enhance the security of watermarking. To show this advantage, the watermark was embedded into the original images with the fractional orders $\alpha = \beta = 0.4$, $\alpha = \beta = 0.9$ and $\alpha = \beta = 0.3$ for FrKMs, FrTMs and FrCMs, respectively. Nevertheless, for watermark extraction, the watermark was extracted with the fractional orders $\alpha = \beta$ varying from 0.1 to 1 by an increment of 0.1. The extracted watermark BER values with various fractional orders are shown in Fig. 5.10. We can conclude from this figure that when incorrect fractional orders are used to extract the watermark, the wrong watermark will be obtained with a BER value of about 0.5. Therefore, the attackers cannot access the embedded watermark without using the correct fractional orders.

5.6 Conclusion

In this chapter, we presented an overview of FrOMs and their applications in image analysis. FrOMs are a useful tool, overcoming and generalizing the classical OMs of integer order. The primary motivation for using them is their additional parameters (fractional orders) where appropriate choices of these parameters can give the best results in applications based on FrOMs. The FrCOMs of Legendre (FrLMs) and the FrDOMs of Charlier (FrCMs) are implemented in this chapter as an example of this type of moments. Applications have been studied to validate the performances of the presented FrOMs, such as 2D/3D image reconstruction, RST invariance, 2D/3D image classification and image watermarking. The experimental results show that

the performances of the FrOMs (FrCOMs and FrDOMs) are superior to those of the classical OMs (COMs and DOMs) in the studied applications.

References

Bibliography

[1] Cave | software: Coil-100: Columbia object image library. https://www1.cs.columbia.edu/cave/software/softlib/coil-100.php. (accessed jan. 03, 2022).

[2] Cvg. http://decsai.ugr.es/cvg/wellcome.html. (accessed jan. 03, 2022).

[3] Mcgill 3d shape benchmar.http://www.cim.mcgill.ca/ shape/benchmark/.(accessed jan. 03, 2022).

[4] I. Batioua, R. Benouini, K. Zenkouar, A. Zahi, and El F. Hakim. 3D image analysis by separable discrete orthogonal moments based on Krawtchouk and Tchebichef polynomials. *Pattern Recognition*, 71:264–277, November 2017.

[5] R. Benouini, I. Batioua, K. Zenkouar, A. Zahi, S. Najah, and H. Qjidaa. Fractional-order orthogonal Chebyshev moments and moment invariants for image representation and pattern recognition. *Pattern Recognition*, 86:332–343, February 2019.

[6] C. Camacho-Bello, C. Toxqui-Quitl, A. Padilla-Vivanco, and J.J. BÃ¡ez-Rojas. High-precision and fast computation of Jacobi-Fourier moments for image description. *JOSA A*, 31(1):124–134, January 2014. Publisher: Optical Society of America.

[7] C.W. Chong, P. Raveendran, and R. Mukundan. The scale invariants of pseudo-Zernike moments. *Pattern Analysis & Applications*, 6(3):176–184, December 2003.

[8] G. Cristobal and V. Marcos. Texture classification using discrete Tchebichef moments. *Journal of the Optical Society of America A*, 30:1580, July 2013.

[9] X.B. Dai, H.Z. Shu, L.M. Luo, G.N. Han, and J.L. Coatrieux. Reconstruction of tomographic images from limited range projections using discrete Radon transform and Tchebichef moments. *Pattern Recognition*, 43(3):1152–1164, March 2010.

[10] A. Daoui, M. Yamni, O. El ogri, H. Karmouni, M. Sayyouri, and H. Qjidaa. Stable computation of higher order Charlier moments for signal and image reconstruction. *Information Sciences: an International Journal*, 521(C):251–276, June

2020.

[11] O. El Ogri, A. Daoui, M. Yamni, H. Karmouni, M. Sayyouri, and H. Qjidaa. New set of fractional-order generalized Laguerre moment invariants for pattern recognition. *Multimedia Tools and Applications*, 79(31):23261–23294, August 2020.

[12] S. Farokhi, U. Ullah Sheikh, J. Flusser, and B. Yang. Near infrared face recognition using Zernike moments and Hermite kernels. *Information Sciences*, 316:234–245, September 2015.

[13] J. Flusser, T. Suk, and B. Zitova. *2D and 3D Image Analysis by Moments*. John Wiley Sons, 2016.

[14] J. Flusser, B. Zitova, and T. Suk. *Moments and moment invariants in pattern recognition*. John Wiley Sons, 2009.

[15] S.H. Friedberg, A.J. Insel, and L.E. Spence. *Linear algebra*. Essex: Pearson, 2014.

[16] A. Hmimid, M. Sayyouri, and H. Qjidaa. Image classification using novel set of charlier moment invariants. *WSEAS Transactions on Signal Processing*, 10:156–167, January 2014.

[17] A. Hmimid, M. Sayyouri, and H. Qjidaa. Image classification using separable invariant moments of Charlier-Meixner and support vector machine. *Multimedia Tools and Applications*, 77(18):23607–23631, September 2018.

[18] K.M. Hosny. Robust template matching using orthogonal Legendre moment invariants. *Journal of Computer Science*, 6, October 2010.

[19] K.M. Hosny. Image representation using accurate orthogonal Gegenbauer moments. *Pattern Recognition Letters*, 32(6):795–804, April 2011.

[20] K.M. Hosny. New set of Gegenbauer moment invariants for pattern recognition applications. *Arabian Journal for Science and Engineering*, 39(10):7097–7107, October 2014.

[21] T. Jahid, A. Hmimid, H. Karmouni, M. Sayyouri, H. Qjidaa, and A. Rezzouk. Image analysis by Meixner moments and a digital filter. *Multimedia Tools and Applications*, 77(15):19811–19831, August 2018.

[22] T. Jahid, H. Karmouni, A. Hmimid, M. Sayyouri, and H. Qjidaa. Image moments and reconstruction by Krawtchouk via Clenshaw's reccurence formula. In *2017 International Conference on Electrical and Information Technologies (ICEIT)*, pages 1–7, November 2017.

[23] T. Jahid, H. Karmouni, M. Sayyouri, A. Hmimid, and H. Qjidaa. Fast algorithm of 3D discrete image orthogonal moments computation based on 3D cuboid. *Journal of Mathematical Imaging and Vision*, 61(4):534–554, May 2019.

[24] E.G. Karakasis, G.A. Papakostas, D.E. Koulouriotis, and V.D. Tourassis. A unified methodology for computing accurate quaternion color moments and moment invariants. *IEEE Transactions on Image Processing*, 23(2):596–611, February 2014. Conference Name: IEEE Transactions on Image Processing.

[25] H. Karmouni, T. Jahid, A. Hmimid, M. Sayyouri, and H. Qjidaa. Fast computation of inverse Meixner moments transform using Clenshaw's formula. *Multimedia Tools and Applications*, 78(22):31245–31265, November 2019.

[26] H. Karmouni, T. Jahid, Z. Lakhili, A. Hmimid, M. Sayyouri, H. Qjidaa, and A. Rezzouk. Image reconstruction by Krawtchouk moments via digital filter. In

2017 Intelligent Systems and Computer Vision (ISCV), pages 1–7, April 2017.

[27] H. Karmouni, T. Jahid, M. Sayyouri, R. El Alami, and H. Qjidaa. Fast 3D image reconstruction by cuboids and 3D Charlier's moments. *Journal of Real-Time Image Processing*, 17(4):949–965, August 2020.

[28] H. Karmouni, T. Jahid, M. Sayyouri, A. Hmimid, and H. Qjidaa. Fast reconstruction of 3D images using Charlier discrete orthogonal moments. *Circuits, Systems, and Signal Processing*, 38(8):3715–3742, August 2019.

[29] B.S. H. Kashkari and M.I. Syam. Fractional-order Legendre operational matrix of fractional integration for solving the Riccati equation with fractional order. *Applied Mathematics and Computation*, 290:281–291, November 2016.

[30] P. Kaur, H.S. Pannu, and A.K. Malhi. Plant disease recognition using fractional-order Zernike moments and SVM classifier. *Neural Computing and Applications*, 31(12):8749–8768, December 2019.

[31] S. Kazem, S. Abbasbandy, and S. Kumar. Fractional-order Legendre functions for solving fractional-order differential equations. *Applied Mathematical Modelling*, 37, April 2013.

[32] M. Kharbat, N. Aouf, A. Tsourdos, and B. White. Robust brightness description for computing optical flow. In *BMVC*, pages 1–10, January 2008.

[33] A. Khotanzad and Y.H. Hong. Invariant image recognition by Zernike moments. *IEEE Transactions on Pattern Analysis and Machine Intelligence*, 12(5):489–497, May 1990. Conference Name: IEEE Transactions on Pattern Analysis and Machine Intelligence.

[34] L. Kvak, M. Schlegel, and J. Sobota. Generalized moments identification by using orthogonal Laguerre polynomials. *Process control 2006*, June 2006. ISBN: 9788071948605.

[35] X. Liu, G. Han, J. Wu, Z. Shao, G. Coatrieux, and H. Shu. Fractional Krawtchouk transform with an application to image watermarking. *IEEE Transactions on Signal Processing*, 65(7):1894–1908, April 2017. Conference Name: IEEE Transactions on Signal Processing.

[36] M. K. Mandal, T. Aboulnasr, and S. Panchanathan. Image indexing using moments and wavelets. *IEEE Transactions on Consumer Electronics*, 42(3):557–565, August 1996. Conference Name: IEEE Transactions on Consumer Electronics.

[37] R. Mukundan, S.-H. Ong, and P.A. Lee. Image analysis by Tchebichef moments. *IEEE transactions on image processing : a publication of the IEEE Signal Processing Society*, 10:1357–64, February 2001.

[38] P. A. M. Oliveira, R. J. Cintra, F. M. Bayer, S. Kulasekera, and A. Madanayake. A discrete Tchebichef transform approximation for image and video coding. *IEEE Signal Processing Letters*, 22(8):1137–1141, August 2015. Conference Name: IEEE Signal Processing Letters.

[39] G.A. Papakostas, Y.S. Boutalis, D.A. Karras, and B.G. Mertzios. Fast numerically stable computation of orthogonal Fourier-Mellin moments. *Computer Vision, IET*, 1:11–16, April 2007.

[40] G.A. Papakostas, Y.S. Boutalis, D.A. Karras, and B.G. Mertzios. Modified factorial-free direct methods for Zernike and Pseudo-Zernike moment computation. *IEEE Transactions on Instrumentation and Measurement*, 58(7):2121–2131, July 2009. Conference Name: IEEE Transactions on Instrumentation and

Measurement.
[41] G.A. Papakostas, E.G. Karakasis, and D.E. Koulouriotis. Accurate and speedy computation of image Legendre moments for computer vision applications. *Image and Vision Computing*, 28(3):414–423, March 2010.
[42] S. Ryu, M. Kirchner, M. Lee, and H. Lee. Rotation invariant localization of duplicated image regions based on Zernike moments. *IEEE Transactions on Information Forensics and Security*, 8(8):1355–1370, August 2013. Conference Name: IEEE Transactions on Information Forensics and Security.
[43] M. Sayyouri, A. Hmimid, H. Karmouni, H. Qjidaa, and A. Rezzouk. Image classification using separable invariant moments of Krawtchouk-Tchebichef. In *2015 IEEE/ACS 12th International Conference of Computer Systems and Applications (AICCSA)*, pages 1–6, November 2015. ISSN: 2161-5330.
[44] M. Sayyouri, A. Hmimid, and H. Qjidaa. Image classification using separable discrete moments of Charlier-Tchebichef. In Abderrahim Elmoataz, Olivier Lezoray, Fathallah Nouboud, and Driss Mammass, editors, *Image and Signal Processing*, Lecture Notes in Computer Science, pages 441–449, Cham, 2014. Springer International Publishing.
[45] M. Sayyouri, A. Hmimid, and H. Qjidaa. A fast computation of novel set of Meixner invariant moments for image analysis. *Circuits, Systems, and Signal Processing*, 34(3):875–900, March 2015.
[46] Y. Sheng and L. Shen. Orthogonal Fourier-Mellin moments for invariant pattern recognition. *JOSA A*, 11(6):1748–1757, June 1994. Publisher: Optical Society of America.
[47] C. Singh and R. Upneja. Accurate calculation of high order pseudo-Zernike moments and their numerical stability. *Digital Signal Processing*, 27:95–106, April 2014.
[48] M.R. Teague. Image analysis via the general theory of moments. *JOSA*, 70(8):920–930, August 1980. Publisher: Optical Society of America.
[49] B. Xiao, L. Li, Y. Li, W. Li, and G. Wang. Image analysis by fractional-order orthogonal moments. *Information Sciences*, 382:135–149, March 2017.
[50] B. Xiao, G. Lu, Y. Zhang, W. Li, and G. Wang. Lossless image compression based on integer discrete Tchebichef transform. *Neurocomputing*, 214:587–593, November 2016.
[51] B. Xiao, J. Luo, X. Bi, W. Li, and B. Chen. Fractional discrete Tchebyshev moments and their applications in image encryption and watermarking. *Information Sciences*, 516:545–559, April 2020.
[52] M. Yamni, A. Daoui, O. El ogri, H. Karmouni, M. Sayyouri, and H. Qjidaa. Influence of Krawtchouk and Charlier moment's parameters on image reconstruction and classification. *Procedia Computer Science*, 148:418–427, January 2019.
[53] M. Yamni, A. Daoui, O. El ogri, H. Karmouni, M. Sayyouri, H. Qjidaa, and J. Flusser. Fractional Charlier moments for image reconstruction and image watermarking. *Signal Processing*, 171:107509, June 2020.
[54] B. Yang and M. Dai. Image reconstruction from continuous Gaussian-Hermite moments implemented by discrete algorithm. *Pattern Recognition*, 45(4):1602–1616, April 2012.
[55] B. Yang, T. Suk, M. Dai, and J. Flusser. 2D and 3D image analysis by Gaussian-

Hermite moments. In George Papakostas, editor, *Gate to Computer Science and Research*, volume 1, pages 143–173. Science Gate Publishing, 1st edition, July 2014.

[56] P.T. Yap, R. Paramesran, and S.H. Ong. Image analysis using Hahn moments. *IEEE transactions on pattern analysis and machine intelligence*, 29:2057–62, December 2007.

[57] P.T. Yap, P. Raveendran, and S.H. Ong. Image analysis by Krawtchouk moments. *IEEE Transactions on Image Processing*, 12:1367–1377, January 2003.

[58] H. Zhang, Z. Li, and Y. Liu. Fractional orthogonal Fourier-Mellin moments for pattern recognition. In Tieniu Tan, Xuelong Li, Xilin Chen, Jie Zhou, Jian Yang, and Hong Cheng, editors, *Pattern Recognition*, Communications in Computer and Information Science, pages 766–778, Singapore, 2016. Springer.

[59] H. Zhu. Image representation using separable two-dimensional continuous and discrete orthogonal moments. *Pattern Recognition*, 45(4):1540–1558, April 2012.

[60] H. Zhu, M. Liu, H. Shu, H. Zhang, and L. Luo. General form for obtaining discrete orthogonal moments. *Image Processing, IET*, 4:335–352, November 2010.

[61] H. Zhu, H. Shu, J. Liang, L. Luo, and J.L. Coatrieux. Image analysis by discrete orthogonal Racah moments. *Signal Processing*, 87(4):687–708, April 2007.

[62] H. Zhu, H. Shu, J. Zhou, L. Luo, and J.L. Coatrieux. Image analysis by discrete orthogonal dual Hahn moments. *Pattern Recognition Letters*, 28(13):1688–1704, 2007.